Switching Model Stein Variational Sampling Filter for Mixed LOS/NLOS Industrial Indoor Positioning

Marco Piavanini, *Graduate Student Member, IEEE*, Mattia Brambilla, *Member, IEEE*, Monica Nicoli, *Senior Member, IEEE*

***Abstract*— Internet of Things (IoT) wireless technologies serve as key enabler for location-based services in emerging applications such as autonomous robotics, industrial automation, augmented and virtual reality. Wide-Band technologies, including Ultra Wide-Band (UWB) and 5G-advanced millimeter-waves, are the preferred solutions in these contexts for their high potentials in precise positioning. A main challenge is the mitigation of radio propagation effects that arise in complex environments, such as in industrial facilities, where frequent blockage events limit the accuracy and integrity of localization services. This article tackles the problem focusing on precise indoor navigation in industrial environments with dense and dynamic blockage conditions. Our proposal relies on an innovative particle filtering technique, based on the Stein Variational Adaptive Importance Sampling (SVA-IS), to improve the sampled representation of the location posterior distribution by integrating prior information on the intermittent visibility-blockage dynamics. We assess the proposed solution through indoor experiments conducted in industrial scenarios using UWB devices. Our results show significant improvements with respect to state of the art filters in terms of both accuracy and robustness of the location tracking.**

***Index Terms*— Indoor navigation, Particle Filters, Stein Variational Gradient Descend, UWB technology**

I. Introduction

Internet of Things (IoT) wireless technologies have become increasingly pervasive in indoor environments, spanning industrial consumer and everyday life applications [1]. As a result, new location-based services are now emerging, particularly in industrial automation use cases such as robot navigation, asset tracking and safety of employees [2]. A number of wireless technologies have been investigated for indoor positioning, including Bluetooth [3], Wi-Fi [4], LoRa [5] and cellular Long Term Evolution (LTE) [6]. More precise solutions are provided by large bandwidth systems, such as millimeter-wave 5G [7], [8] and Ultra Wide-Band (UWB) [9], [10], [11]. While 5G-advanced is emerging with high potentials in the long term, UWB is now a mature technology that has been successfully employed in several localization scenarios [12], [13]. Commercial UWB positioning systems exploit various ranging measurements including Time Difference of Arrival (TDoA) [14], [15] and Two Way Ranging (TWR) [16], [17], angular measurements [18], [19], and fingerprinting based on received signal power [20], [21].

Bayesian filters are commonly implemented to augment the localization performances, relying on non-linear variants of the Kalman Filter (KF), such as the Extended Kalman Filter (EKF) [22], the Unscented Kalman Filter (UKF) [23], the Cubature Kalman Filter (CKF) [24] and the posterior linearization filter [25]. Particle Filters (PFs) [26], [27] can be more accurate at the cost of a higher computational load, while new methods based on the Stein Variational Gradient Descent (SVGD) framework [28], [29], [30], such as the Stein Particle Filter (SPF) [31] and the Annealed Stein Particle Filter (A-SPF) [32], improve the sampled representation of the location Probability Density Functions (PDFs) enhancing the tracking performance, in particular when multi-modal PDFs are considered.

A major issue in industrial environments is Non-Line of Sight (NLOS) caused by obstacles such as machineries, walls and robots. Human workers may also significantly attenuate the UWB direct path caused by the human body [33], generating a non-static and varying over time NLOS condition [34], [35]. Taking advantage of advanced processing techniques, NLOS detection and mitigation [36], [37] has been recently taken up to improve the localization and communication performance, leveraging the full Channel Impulse Response (CIR) for statistical characterization [38] or by means of machine learning algorithms [39], [40], [41]. Although promising, these solutions have the limit of requiring the processing of raw CIR data, which might not be easily accessible in commercial devices. As an alternative, robust Bayesian filtering methods [42] treat NLOS measurements as outliers, but they may be ineffective if the blockage condition persists, as they do not incorporate statistical information about NLOS propagation. Another possibility is to embed into the Bayesian filters a statistical characterization of the dynamics of the Line of Sight (LOS)/NLOS conditions, based on prior map information [43], skewed and heavy-tailed distributions [44], [45], mixture models [46], or switching Markov models. For the latter case, solutions have been developed using Interacting Multiple Model (IMM) filtering [47], Switching Model Parti-

M. Piavanini and M. Brambilla are with Dipartimento di Elettronica, Informazione e Bioingegneria (DEIB), Politecnico di Milano, 20133 Milan, Italy (e-mail: {marco.piavanini, mattia.brambilla}@polimi.it).

M. Nicoli is with Dipartimento di Ingegneria Gestionale (DIG), Politecnico di Milano, 20133 Milan, Italy (e-mail: monica.nicoli@polimi.it).

cle Filter (SM-PF) [48], [49] and Rao-Blackwellized Particle Filter (RBPF) [50], [51]. Yet, these methods rely on simplified PDF assumptions and approximations, which may reduce the positioning accuracy in dense multipath scenarios with location ambiguities.

In this paper, we propose a new tracking framework that targets to improve the positioning performance in indoor scenarios with dense multipath and mixed LOS/NLOS conditions, providing a more reliable representation of the blockage statistics and the position belief. For modeling the blockage statistics, we build upon the work in [49] to propose a novel tracking filter that improves the previously developed SM-PF solution in terms of positioning accuracy and robustness. The proposed filter, named Switching Model Stein Variational Sampling Filter (SM-SVSF), is rooted in the sampling theory of the PF framework. Unlike standard PF and RBPF, which sample from a suboptimal proposal distribution, our proposed filter is designed to sample from the optimal proposal distribution with minimal approximation. To achieve this goal, we build on the SVGD framework and specifically utilize the Stein Variational Adaptive Importance Sampling (SVA-IS) algorithm [52], which enables the deterministic generation of a set of independent and identically distributed (i.i.d) samples from a target distribution. The proposed filter is designed to directly work with the TDoA measurements extracted from commercial UWB device. To assess the method performance, we carry out two experimental campaigns with UWB devices in industrial indoor environments where we record raw TDoA data and use them to evaluate the performances offline. We compare our tracking filter with the former SM-PF described in [49], showing that our novel solution provides both accuracy and robustness augmentation.

The paper is organized as follows: in Section II we introduce the system model and the filtering framework; in Section III we present the proposed SM-SVSF algorithm; in Section IV we describe the industrial indoor experiments; in Section V we discuss the conclusion and directions for future research.

Notation: bold letters indicate column vectors belonging to the real number set $\mathbb{R}$ or the natural number set $\mathbb{N}$. The identity matrix of dimension $M \times M$ is indicated as $\mathbf{I}_M$. The Gaussian probability density function of a random variable x is defined as $\mathcal{N}(x; \mu, \sigma^2)$ where μ is the mean value and σ is the standard deviation. The exponential distribution with rate parameter λ is defined as $\mathcal{E}(\lambda)$, the Exponentially Modified Gaussian distribution as $\mathcal{EN}(x; \mu, \sigma^2, \lambda)$ and the Laplace Normal distribution as $\mathcal{LN}(x; \mu, \sigma^2, \lambda)$ where μ, σ and λ are the mean value, the standard deviation and the rate parameter, respectively.

II. System Model

In this section, we first introduce the model for tracking in mixed LOS/NLOS visibility condition (Section II-A); then, we highlight the Bayesian framework employed for the filter design (Section II-B); lastly, we provide an overview of the SVA-IS algorithm (Section II-C), which is a fundamental theory used for our SM-SVSF proposal.

A. Localization model

Consider an UWB network with N static Access Points (APs) acting as anchors and deployed at known position $\mathbf{s}_i = [s_{x,i} \; s_{y,i}]^{\mathrm{T}}$, with $i = 1, \ldots, N$. The aim of the UWB network is to estimate the 2-D position at time t of a tag periodically broadcasting UWB signals. Denote with $\mathbf{x}_t$ the 2-D tag's position (or location) at time $t = 1, \ldots, T$, the following dynamic model is considered:

$$\mathbf{x}_t = \mathbf{x}_{t-1} + \Delta t \, \mathbf{w}_t, \tag{1}$$

where Δt is the sampling interval and $\mathbf{w}_t$ is a zero mean Gaussian random variable with covariance $\mathbf{Q}_t$, which accounts for the motion model uncertainty.

The UWB signal propagation from the tag to each AP can be subject to LOS or NLOS conditions. In the case of NLOS, the time-of-flight measurement is biased, leading to localization errors. Building on the methodology outlined in [49], we propose to mitigate the NLOS-related biases by jointly tracking the location and the dynamics of the sight condition modeled as a switching variable $\mathbf{m}_t = [m_t^{(1)} \cdots m_t^{(N)}]^{\mathrm{T}} \in \{0, 1\}^N$, where $m_t^{(i)} = 0$ if the i-th AP is in LOS, and $m_t^{(i)} = 1$ if it is in NLOS. The sight condition evolution over time is ruled by a first order Markov chain with transition probability

$$p(\mathbf{m}_t | \mathbf{m}_{t-1}) = \prod_{i=1}^{N} p(m_t^{(i)} = a | m_{t-1}^{(i)} = b), \tag{2}$$

where $p(m_t^{(i)} = a | m_{t-1}^{(i)} = b)$ is the probability that AP i switches from state $a = \{0, 1\}$ to state $b = \{0, 1\}$. The Markov chain with transition probabilities defined in (2) models the changes in each AP's sight condition as independent from the others. While this does not thoroughly represent the variations in the propagation environment, where sight transitions can depend on the AP positions, building structure, and user location, it has the advantage of not requiring any knowledge of the building structure nor map information.

A typical positioning approach used by UWB systems to avoid tag synchronization is to rely on TDoA measurements. The TDoA is computed as the difference of pseudo-ranges between anchor pair $\{i, k\}$, where the k-th anchor is the reference anchor (also called master AP). Without loss of generality, here we assume $k = 1$. We also assume perfect synchronization between APs. The pseudo-range of the i-th AP, indicated with $\rho_t^{(i)}$, is modeled as:

$$\rho_t^{(i)} = d_t^{(i)} + m_t^{(i)} \tau_i + n_i(m_t^{(i)}), \tag{3}$$

where $d_t^{(i)} = \|\mathbf{x}_t - \mathbf{s}_i\|$ is the true distance between the tag and the AP and $\tau_i \sim \mathcal{E}(\lambda)$ is an exponential random variable with rate parameter $\lambda > 0$, $n_i(m_t^{(i)})$ is a Gaussian random variable modeling the visibility-dependent measurement uncertainty. The exponential random variable τ_i models the excess delay introduced in the pseudo-range measurement when the AP is in NLOS condition ($m_t^{(i)} = 1$) [53], while in LOS ($m_t^{(i)} = 0$) the contribution is zero. The Gaussian noise is defined as $n_i(m_t^{(i)} = 0) \sim \mathcal{N}(n_i; 0, \sigma^2_{\mathrm{LOS}})$ if the AP is in LOS, otherwise $n_i(m_t^{(i)} = 1) \sim \mathcal{N}(n_i; 0, \sigma^2_{\mathrm{NLOS}})$. The TDoA measurement is

TABLE I: Distribution of the measurement noise for different sight conditions

$m_t^{(i)}$	$m_t^{(k)}$	$p_{\widetilde{n}_i}(\widetilde{n}_i)$
0	0	$\mathcal{N}(\widetilde{n}_i; 0, 2\sigma^2_{\text{LOS}})$
0	1	$\mathcal{EN}(\widetilde{n}_i; 0, \sigma^2_{\text{LOS}} + \sigma^2_{\text{NLOS}}, \lambda)$
1	0	$\mathcal{EN}(\widetilde{n}_i; 0, \sigma^2_{\text{LOS}} + \sigma^2_{\text{NLOS}}, \lambda)$
1	1	$\mathcal{LN}(\widetilde{n}_i; 0, 2\sigma^2_{\text{NLOS}}, \lambda)$

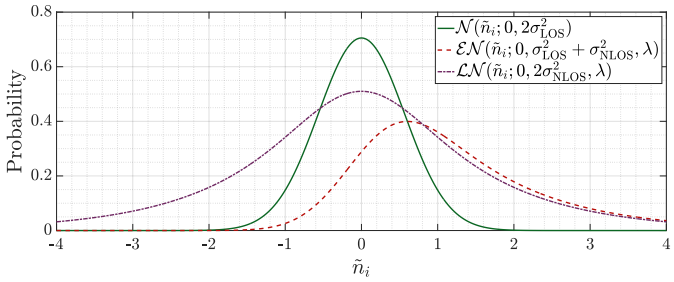

Fig. 1: Graphical comparison of noise distribution. Parameters are set as follows: σ_{LOS} = 0.4, σ_{NLOS} = 0.4 and $\lambda = 0.8$.

computed as:

$$y_t^{(i)} = \rho_t^{(i)} - \rho_t^{(k)} = d_t^{(i)} - d_t^{(k)} + \widetilde{n}_i, \tag{4}$$

with noise term

$$\widetilde{n}_i = m_t^{(i)}\tau_i - m_t^{(k)}\tau_k + n_i(m_t^{(i)}) - n_i(m_t^{(k)}). \tag{5}$$

The PDF of the noise in (5), indicated by $p_{\widetilde{n}_i}(\widetilde{n}_i)$, depends on the LOS/NLOS conditions of the i-th AP and the reference anchor k, i.e., τ_i and τ_k, as well as on the measurement noise terms $n_i(m_t^{(i)})$ and $n_i(m_t^{(k)})$. If both APs are in LOS, the distribution of $\widetilde{n}_i$ is Gaussian. If one AP is in NLOS, the noise is the sum of a Gaussian-distributed and an exponential-distributed random variables, which leads to an Exponentially Modified Gaussian (EMG) distribution. If both APs are in NLOS, the PDF follows a Laplace Normal (LN) distribution. We summarize in Table I the possible distributions of the measurement noise, whereas in Fig. 1 we compare the Gaussian, EMG and LN distributions.

All the TDoA measurements collected by N anchors are modeled as:

$$\mathbf{y}_t = \mathbf{h}_t(\mathbf{x}_t) + \widetilde{\mathbf{n}}(\mathbf{m}_t), \tag{6}$$

where $\mathbf{h}_t(\mathbf{x}_t) = [d_t^{(2)} - d_t^{(1)} \cdots d_t^{(N)} - d_t^{(1)}]^{\text{T}}$ and $\widetilde{\mathbf{n}}(\mathbf{m}_t) = [\widetilde{n}_2 \cdots \widetilde{n}_N]^{\text{T}}$. Based on the motion model (1), the sight condition transition model (2), and the measurement model (6), the positioning problem results in a Markov switching State Space Model (SSM) with non-linear non-Gaussian dynamics. Its graphical representation is reported in Fig. 2, which remarks the independency between the sight condition and location chains, while the measurements $\mathbf{y}_t$ depend on both the current sight condition $\mathbf{m}_t$ and location $\mathbf{x}_t$. In our model, we assume the sight condition $\mathbf{m}_t$ is independent from the location $\mathbf{x}_t$. This assumption allows an easier and more flexible description of the sight condition evolution in time.

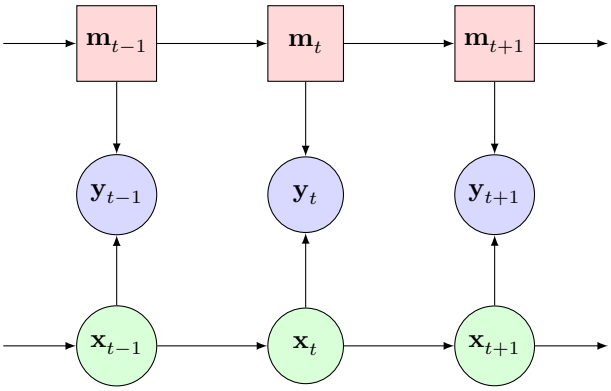

Fig. 2: Visualization of the Markov switching SSM.

B. Bayesian tracking framework

For tracking the location-sight state we propose to employ the PF framework for switching systems [26], [48]. which sequentially computes the posterior PDF $p(\mathbf{x}_{1:t}, \mathbf{m}_{1:t}|\mathbf{y}_{1:t})$, where $\mathbf{x}_{1:t}$, $\mathbf{m}_{1:t}$ and $\mathbf{y}_{1:t}$ denote the states (locations), sight conditions, and measurements up to time t, respectively. Assuming Markovian properties of location and sight condition, according to the model in Section II-A, the posterior PDF can be factorized as in (7), where $p(\mathbf{x}_{1:t}, \mathbf{m}_{1:t}, \mathbf{y}_{1:t})$ is referred here as the *unnormalized* posterior PDF [26]. The PDF in (7) depends on the transition PDFs of the location and the sight conditions, a normalization constant $p(\mathbf{y}_{1:t})$ and the likelihood of the TDoA measurements

$$p(\mathbf{y}_t|\mathbf{x}_t, \mathbf{m}_t) = \prod_{i=2}^{N} p(y_t^{(i)}|\mathbf{x}_t, m_t^{(i)}, m_t^{(k)}) \tag{8}$$

defined as the product of $N-1$ individual likelihoods evaluated as:

$$p(y_t^{(i)}|\mathbf{x}_t, m_t^{(i)}, m_t^{(k)}) = p_{\widetilde{n}_i}(y_t - h_i(\mathbf{x}_t)). \tag{9}$$

The posterior PDF in (7) depends on the unnormalized posterior distribution at time $t-1$. Given that the normalization constant is $p(\mathbf{y}_{1:t}) = p(\mathbf{y}_t|\mathbf{y}_{1:t-1})p(\mathbf{y}_{1:t-1})$, the posterior PDF can be recursively defined as:

$$p(\mathbf{x}_{1:t}, \mathbf{m}_{1:t}|\mathbf{y}_{1:t}) \propto \frac{p(\mathbf{x}_{1:t-1}, \mathbf{m}_{1:t-1}|\mathbf{y}_{1:t-1})}{p(\mathbf{y}_t|\mathbf{y}_{1:t-1})}. \tag{10}$$

Following the PF approach, our aim is to sample a set of particles $\{\mathbf{x}_{1:t}^{(j)}, \mathbf{m}_{1:t}^{(j)}\}_{j=1}^{N_p}$ from a proposal distribution $q(\mathbf{x}_{1:t}, \mathbf{m}_{1:t}, \mathbf{y}_{1:t})$ and weight each of them with the (unnormalized) importance weight:

$$w_t^{(j)} = \frac{p(\mathbf{x}_{1:t}^{(j)}, \mathbf{m}_{1:t}^{(j)}, \mathbf{y}_{1:t})}{q(\mathbf{x}_{1:t}^{(j)}, \mathbf{m}_{1:t}^{(j)}, \mathbf{y}_{1:t})}. \tag{11}$$

The proposal distribution is chosen so that it can be recursively constructed:

$$q(\mathbf{x}_{1:t}, \mathbf{m}_{1:t}, \mathbf{y}_{1:t}) = q(\mathbf{x}_t, \mathbf{m}_t|\mathbf{x}_{1:t-1}, \mathbf{m}_{1:t-1}, \mathbf{y}_{1:t}) q(\mathbf{x}_{1:t-1}, \mathbf{m}_{1:t-1}, \mathbf{y}_{1:t-1}). \tag{12}$$

The recursive estimate of the probability distribution implies the availability of the set of particles $\{\mathbf{x}_{1:t-1}^{(j)}, \mathbf{m}_{1:t-1}^{(j)}\}_{j=1}^{N_p}$ from the past posterior, so obtaining samples from (12) at

$$p(\mathbf{x}_{1:t}, \mathbf{m}_{1:t}|\mathbf{y}_{1:t}) = \frac{p(\mathbf{x}_{1:t}, \mathbf{m}_{1:t}, \mathbf{y}_{1:t})}{p(\mathbf{y}_{1:t})} = \frac{p(\mathbf{x}_t|\mathbf{x}_{t-1})p(\mathbf{m}_t|\mathbf{m}_{t-1})p(\mathbf{y}_t|\mathbf{x}_t, \mathbf{m}_t)p(\mathbf{x}_{1:t-1}, \mathbf{m}_{1:t-1}, \mathbf{y}_{1:t-1})}{p(\mathbf{y}_{1:t})} \tag{7}$$

time t only requires the sampling of the current location and sight condition as:

$$\{\mathbf{x}_t^{(j)}, \mathbf{m}_t^{(j)}\} \sim q(\mathbf{x}_t, \mathbf{m}_t|\mathbf{x}_{1:t-1}^{(j)}, \mathbf{m}_{1:t-1}^{(j)}, \mathbf{y}_{1:t}), \quad \forall\, j = 1, \ldots, N_p. \tag{13}$$

Considering the unnormalized posterior $p(\mathbf{x}_{1:t}, \mathbf{m}_{1:t}, \mathbf{y}_{1:t})$ and (12), the unnormalized importance weights in (11) can then be recursively computed $\forall j = 1, \ldots, N_p$ as:

$$w_t^{(j)} = \frac{p(\mathbf{x}_t^{(j)}|\mathbf{x}_{t-1}^{(j)})p(\mathbf{m}_t^{(j)}|\mathbf{m}_{t-1}^{(j)})p(\mathbf{y}_t|\mathbf{x}_t^{(j)}, \mathbf{m}_t^{(j)})}{q(\mathbf{x}_t^{(j)}, \mathbf{m}_t^{(j)}|\mathbf{x}_{1:t-1}^{(j)}, \mathbf{m}_{1:t-1}^{(j)}, \mathbf{y}_{1:t})} w_{t-1}^{(j)}, \tag{14}$$

where $w_{t-1}^{(j)}$ is the unnormalized importance weight at time $t-1$ computed as the ratio of $p(\mathbf{x}_{1:t-1}^{(j)}, \mathbf{m}_{1:t-1}^{(j)}, \mathbf{y}_{1:t-1})$ and $q(\mathbf{x}_{1:t-1}^{(j)}, \mathbf{m}_{1:t-1}^{(j)}, \mathbf{y}_{1:t-1})$.

In general, sampling directly from (13) is infeasible. A classic approach is to use the transition probability as proposal distribution, i.e.,

$$q(\mathbf{x}_t, \mathbf{m}_t|\mathbf{x}_{1:t-1}, \mathbf{m}_{1:t-1}, \mathbf{y}_{1:t}) = p(\mathbf{x}_t|\mathbf{x}_{t-1})p(\mathbf{m}_t|\mathbf{m}_{t-1}), \tag{15}$$

resulting in the bootstrap filter [26], in which the importance weights are proportional to the likelihood probabilities. With bootstrap PF, we can sample independently from the transition probabilities of the location and the sight condition, whereas the importance weights in (11) become proportional to the likelihood. After the sampling step, a resampling algorithm is applied to prevent particle degeneracy. The most common resampling algorithm is the systematic resampling [54]. Other approaches can rely on evolutionary algorithms to prevent particle degeneracy [55]. Bootstrap filters can lead to poor performance since they do not sample from the optimal proposal distribution [26].

C. SVA-IS overview

We recall here the SVGD and SVA-IS methodologies used to approximate the posterior PDF. For simplicity, we omit the time index t and denote $\mathbf{x}_t$ as $\mathbf{x}$, $\mathbf{x}_t^{(j)}$ as $\mathbf{x}_j$ and $w_t^{(j)}$ as w_j. The SVGD [28] is a non-parametric, deterministic algorithm for approximating a PDF $p(\mathbf{x})$, where $\mathbf{x} \in \mathbb{R}^{\mathrm{M}}$ and the PDF can be expressed as:

$$p(\mathbf{x}) = \gamma^{-1} p_u(\mathbf{x}). \tag{16}$$

In (16), $p_u(\mathbf{x})$ is referred to as unnormalized PDF while γ is a normalization constant. The goal of SVGD is to deterministically transport a set of initial particles $\boldsymbol{\chi}_0 = \{\mathbf{x}_j^{(0)}\}_{j=1}^{N_p}$ towards the target distribution by iteratively applying a non-linear transformation:

$$\mathbf{x}_j^{(\ell)} = \mathbf{x}_j^{(\ell-1)} + \varepsilon\, \boldsymbol{\phi}_\ell(\mathbf{x}_j^{(\ell-1)}), \tag{17}$$

where ε is the step size and $\ell = 1, \ldots, L$ is the iteration step. The optimal non-linear transformation $\boldsymbol{\phi}_\ell^*$ (also called direction) is chosen such that it minimizes the Kullback-Leibler (KL) divergence between the approximated PDF

$$\widehat{p}(\mathbf{x}) = \frac{1}{N_p} \sum_{\mathbf{x}_j^{(\ell)} \in \mathcal{X}_\ell} \delta(\mathbf{x} - \mathbf{x}_j^{(\ell)}) \tag{18}$$

and the target distribution $p(\mathbf{x})$, leading to:

$$\boldsymbol{\phi}_\ell^* = \underset{\boldsymbol{\phi}_\ell \in \boldsymbol{\Phi};\, ||\boldsymbol{\phi}_\ell|| \leq 1}{\arg\max} \left(-\frac{d}{d\varepsilon} \mathrm{KL}\big(\widehat{p}(\mathbf{x})||p(\mathbf{x})\big) \right), \tag{19}$$

where $\boldsymbol{\Phi}$ is the functional space of the function $\boldsymbol{\phi}_\ell^*$. As proved in [28], a closed-form solution for (19) exists if the functional space is the unit ball of a vector-valued Reproducing Kernel Hilbert Space (RKHS) with an associated positive kernel $\mathcal{K}(\cdot, \cdot)$. Computing the optimal direction requires evaluating the Stein Discrepancy (SD) [29] over the domain of $\mathbf{x} \in \mathbb{R}^{\mathrm{M}}$. Since we are using approximated distribution, the optimal direction can be computed using the set of particles as follows:

$$\boldsymbol{\phi}_\ell^*(\mathbf{x}_j^{\ell-1}) = \frac{1}{N_p} \sum_{\mathbf{x} \in \mathcal{X}_{\ell-1}} \mathcal{K}(\mathbf{x}, \mathbf{x}_j^{(\ell-1)}) \nabla_{\mathbf{x}} \log p(\mathbf{x}) + \nabla_{\mathbf{x}} \mathcal{K}(\mathbf{x}, \mathbf{x}_j^{(\ell-1)}). \tag{20}$$

The term $\mathcal{K}(\mathbf{x}, \mathbf{x}_j^{(\ell-1)}) \nabla_{\mathbf{x}} \log p(\mathbf{x})$ in (20) acts as a driving force that pushes the particles into high-density regions of the PDF, while the term $\nabla_{\mathbf{x}} \mathcal{K}(\mathbf{x}, \mathbf{x}_j^{(\ell-1)})$ serves as a repulsive force, promoting exploration of the possible modes of the PDF.

The SVGD algorithm can be further transformed with a standard Importance Sampling (IS) algorithm, namely the SVA-IS, with the modification introduced in [52]. The SVA-IS algorithm is a powerful algorithm for sampling distributions. It exploits the property that the KL divergence between $\widehat{p}(\mathbf{x})$ and $p(\mathbf{x})$ is monotonically decreasing [52], [29]: as the number of iterations increases, the approximation of $p(\mathbf{x})$ improves, leading to samples that more accurately represent the original distribution. Moreover, if the size of the chosen set is carefully decided, the algorithm can accurately sample from the PDF and be also computationally efficient. To perform IS, the set of particles $\mathcal{X}_\ell$ is divided into two subsets: the master particles $\mathcal{M}_\ell = \{\mathbf{x}_j^{(\ell)}\}_{j=1}^{N_m}$ and the follower particles $\mathcal{F}_\ell = \mathcal{X}_\ell \setminus \mathcal{M}_\ell$. In this framework, only the master particles are used to compute the non-linear transformation in (20) (instead of using the whole set of particles), allowing to rewrite (20) as:

$$\boldsymbol{\phi}_\ell^*(\mathbf{x}_j^{\ell-1}) = \frac{1}{N_p} \sum_{\mathbf{x} \in \mathcal{M}_{\ell-1}} \mathcal{K}(\mathbf{x}, \mathbf{x}_j^{(\ell-1)}) \nabla_{\mathbf{x}} \log p(\mathbf{x}) + \nabla_{\mathbf{x}} \mathcal{K}(\mathbf{x}, \mathbf{x}_j^{(\ell-1)}). \tag{21}$$

By constructing the optimal direction using master particles and iteratively transforming the follower particles, we can generate i.i.d. samples from the distribution in (18). At the

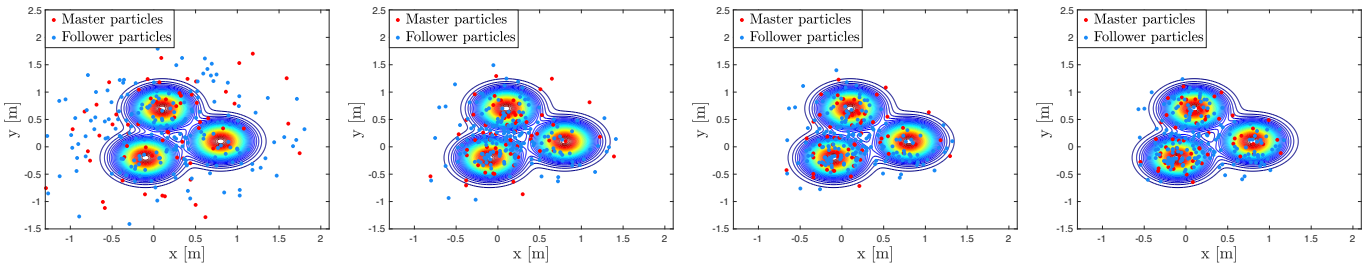

(a) (b) (c) (d)

Fig. 3: Evolution of master and follower particles through iterations of an SVA-IS with $N_A = 64$ and $N_p = 256$. Four iterations are represented: (a) $\ell = 1$, (b) $\ell = 10$, (c) $\ell = 20$ and (d) $\ell = L$.

end of this process, we obtain the samples $\mathbf{x}_j^{(L)} \in \mathcal{F}_L$ with corresponding weights $\alpha(\mathbf{x}_j^{(L)})$. The weights of the proposal distribution are iteratively updated as:

$$\alpha(\mathbf{x}_j^{(\ell)}) = \alpha(\mathbf{x}_j^{(\ell-1)}) \left| \det \left(\mathbf{I}_M + \varepsilon \nabla_{\mathbf{x}} \boldsymbol{\phi}_\ell^*(\mathbf{x}_j^{\ell-1}) \right) \right|^{-1}. \quad (22)$$

Finally, the (unnormalized) importance weights can be computed on the follower set of particles:

$$w_j = \frac{p_u(\mathbf{x}_j^{(L)})}{\alpha(\mathbf{x}_j^{(L)})}, \quad \forall \mathbf{x}_j^{(L)} \in \mathcal{F}_L. \quad (23)$$

We summarize the SVA-IS steps in Algorithm 1, while Fig. 3 highlights the evolution of the master and follower particles in the approximation and sampling of a Gaussian mixture PDF. Notably, the red dots, representing master particles, provide a more accurate PDF approximation, resulting in better sampled follower particles.

III. Proposed SM-SVSF

In this section, we propose a new filter, referred to as SM-SVSF, to track the location jointly with the NLOS dynamics so as to mitigate the location bias. Recalling Section II-B, we aim to generate samples of the location and sight condition from (13). Using the transition probability as proposal, as in (15), is a suboptimal approach. Therefore, our objective is to sample directly from the optimal proposal distribution with minimal approximation. The optimal proposal distribution is:

$$q(\mathbf{x}_t, \mathbf{m}_t | \mathbf{x}_{1:t-1}, \mathbf{m}_{1:t-1}, \mathbf{y}_{1:t}) = p(\mathbf{x}_t, \mathbf{m}_t | \mathbf{x}_{1:t-1}, \mathbf{m}_{1:t-1}, \mathbf{y}_{1:t}). \quad (24)$$

Algorithm 1: SVA-IS

Input: Initial set of particles $\mathcal{X}_0$
Divide $\mathcal{X}_0$ in $\mathcal{M}_0$ and $\mathcal{F}_0$
for $\ell = 1, \ldots, L$ **do**
  Compute $\nabla_{\mathbf{x}} \log p(\mathbf{x}) \ \ \forall \mathbf{x} \in \mathcal{M}_{\ell-1}$
  Compute $\mathbf{x}_j^{(\ell)}$ using (21) $\ \forall \mathbf{x}_j^{(\ell-1)} \in \mathcal{M}_{\ell-1} \cup \mathcal{F}_{\ell-1}$
  Compute weights $\alpha(\mathbf{x}_j^{(\ell)})$ using (22) $\forall \mathbf{x}_j^{(\ell)} \in \mathcal{F}_\ell$
end
Compute unnormalized importance weights with (23)
Result: i.i.d. samples $\mathcal{F}_L$ with weights $\{w_j\}_{j=1}^{N_p - N_m}$

The PDF in (24) is considered optimal because it minimizes the KL divergence, which is mathematically equivalent to maximizing the Evidence Lower Bound (ELBO), between the recursive proposal in (12) and the posterior PDF in (7) [56]. Taking into account the modeling in Section II-A, the optimal distribution in (24) can be written as:

$$p(\mathbf{x}_t, \mathbf{m}_t | \mathbf{x}_{1:t-1}, \mathbf{m}_{1:t-1}, \mathbf{y}_{1:t}) = \underbrace{\frac{p(\mathbf{y}_t | \mathbf{x}_t, \mathbf{m}_t) p(\mathbf{x}_t | \mathbf{x}_{t-1})}{p(\mathbf{y}_t | \mathbf{x}_{1:t-1}, \mathbf{m}_{1:t-1}, \mathbf{y}_{1:t-1})}}_{r(\mathbf{x}_t, \mathbf{y}_t | \mathbf{m}_t)} p(\mathbf{m}_t | \mathbf{m}_{t-1}). \quad (25)$$

Notice that the optimal proposal distribution is factorized in the sight conditions transition probability $p(\mathbf{m}_t | \mathbf{m}_{t-1})$ and the PDF $r(\mathbf{x}_t, \mathbf{y}_t | \mathbf{m}_t)$. In standard PF settings, sampling from the optimal distribution is intractable due to the unfeasible computation of $r(\mathbf{x}_t, \mathbf{y}_t | \mathbf{m}_t)$. To overcome this issues, we propose a method to draw samples from the optimal proposal distribution using SVA-IS. Fig. 4 shows the ELBO evaluation when sampling using SVA-IS from the optimal PDF, compared to sampling from the transition PDF. As expected, ELBO values obtained with SVA-IS consistently increase and surpass those achieved with standard sampling. Starting from a set of

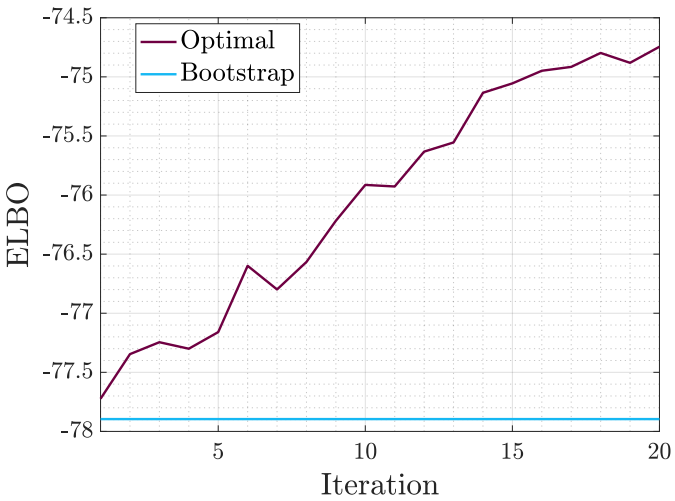

Fig. 4: ELBO evaluation with sampling from the optimal proposal and the standard bootstrap filter.

particles $\{\mathbf{x}_{t-1}^{(j)}, \mathbf{m}_{t-1}^{(j)}\}_{j=1}^{N_p}$ consisting in the solution at time $t-1$, we first sample the sight conditions from the transition probability $\mathbf{m}_t^{(j)} \sim p(\mathbf{m}_t|\mathbf{m}_{t-1}^{(j)})$; then we sample the new particles $\mathbf{x}_t^{(j)} \sim r(\mathbf{x}_t, \mathbf{y}_t|\mathbf{m}_t^{(j)})$ using SVA-IS algorithm obtaining samples from the optimal probability distribution. Notice that we can sample directly from $r(\mathbf{x}_t, \mathbf{y}_t|\mathbf{m}_t)$ using SVA-IS since the log-gradient

$$\nabla_{\mathbf{x}_t} \log r(\mathbf{x}_t, \mathbf{y}_t|\mathbf{m}_t^{(j)}) = \nabla_{\mathbf{x}_t} \log p(\mathbf{y}_t|\mathbf{x}_t, \mathbf{m}_t^{(j)}) + \nabla_{\mathbf{x}_t} \log p(\mathbf{x}_t|\mathbf{x}_{t-1}), \tag{26}$$

can be analytically computed. However, the computation of the gradient can be numerically unstable, to a large extent when the likelihood PDF is sharply peaked. To prevent exploding gradients, a simple yet effective solution is to use gradient clipping. If the magnitude of the gradient exceeds a certain threshold η, the gradient is computed as:

$$\nabla_{\mathbf{x}_t} \log r(\mathbf{x}_t, \mathbf{y}_t|\mathbf{m}_t^{(j)}) = \eta \frac{\nabla_{\mathbf{x}_t} \log r(\mathbf{x}_t, \mathbf{y}_t|\mathbf{m}_t^{(j)})}{||\nabla_{\mathbf{x}_t} \log r(\mathbf{x}_t, \mathbf{y}_t|\mathbf{m}_t^{(j)})||}, \tag{27}$$

which prevents to have large gradient value by limiting its magnitude to $[0, \eta]$.

By using the SVA-IS algorithm, we obtain $N_p - N_m$ i.i.d. particles $\mathbf{x}_t^{(j)}$ with associated weights $\alpha(\mathbf{x}_t^{(j)})$, which are sampled from a PDF that is progressively close to the PDF $r(\mathbf{x}_t, \mathbf{y}_t|\mathbf{m}_t)$ after each iteration. This implies that we acquire particles $\mathbf{x}_t^{(j)}$ from the follower set with the corresponding sight condition $\mathbf{m}_t^{(j)}$ and weights

$$q(\mathbf{x}_t^{(j)}, \mathbf{m}_t^{(j)}|\mathbf{x}_{1:t-1}^{(j)}, \mathbf{m}_{1:t-1}^{(j)}, \mathbf{y}_{1:t}) = \alpha(\mathbf{x}_t^{(j)}) p(\mathbf{m}_t^{(j)}|\mathbf{m}_{t-1}^{(j)}) \tag{28}$$

which closely approximate the optimal posterior. Then, we can compute the unnormalized importance weights $\forall\, j \in \mathcal{F}_L$ as:

$$w_t^{(j)} = \frac{p(\mathbf{x}_t^{(j)}|\mathbf{x}_{t-1}^{(j)}) p(\mathbf{m}_t^{(j)}|\mathbf{m}_{t-1}^{(j)}) p(\mathbf{y}_t|\mathbf{x}_t^{(j)}, \mathbf{m}_t^{(j)})}{\alpha(\mathbf{x}_t^{(j)}) p(\mathbf{m}_t^{(j)}|\mathbf{m}_{t-1}^{(j)})} w_{t-1}^{(j)}. \tag{29}$$

In (29), the term $p(\mathbf{m}_t^{(j)}|\mathbf{m}_{t-1}^{(j)})$ appears both at the numerator and the denominator so it is automatically eluded. Using the unnormalized importance weights in (29), we can now estimate the tag position as:

$$\widehat{\mathbf{x}}_t = \sum_{j=1}^{N_p - N_m} \left(\frac{w_t^{(j)}}{\sum_{j=1} w_t^{(j)}} \right) \mathbf{x}_t^{(j)}. \tag{30}$$

The computation of the unnormalized importance weights in (29) can be numerical unstable especially if the values of $\alpha(\mathbf{x}_t^{(j)})$ are very small. To solve this issue, a solution is to perform weight computation in (22) and (29) in the log domain as:

$$\alpha(\mathbf{x}_j^{(\ell)}) = \alpha(\mathbf{x}_j^{(\ell-1)}) - \log\left(\left| \det\left(\mathbf{I}_M + \varepsilon \nabla_{\mathbf{x}} \boldsymbol{\phi}_\ell^*(\mathbf{x}_j^{\ell-1}) \right) \right| \right), \tag{31}$$

$$w_t^{(j)} = \log(p(\mathbf{x}_t^{(j)}|\mathbf{x}_{t-1}^{(j)})) + \log(p(\mathbf{y}_t|\mathbf{x}_t^{(j)}, \mathbf{m}_t^{(j)})) - \alpha(\mathbf{x}_t^{(j)}) + \log(w_{t-1}^{(j)}). \tag{32}$$

Moreover, the normalization of the weights performed in (30) can be calculated using the LogSumExp (LSE) method to further improve numerical stability [57]. The last step of the tracking filter is resampling. We use systematic resampling algorithm obtaining a novel set of particles $\{\mathbf{x}_t^{(j)}, \mathbf{m}_t^{(j)}\}_{j=1}^{N_p}$ from the set $\mathcal{F}_L$ with equally distributed weights (non-evaluated particles in $\mathcal{M}_L$ are simply discarded). The resampling operation is executed if the Effective Sample Size (ESS), computed as:

$$\text{ESS} = \left(\sum_{j=1}^{N_p - N_m} \left(\frac{w_t^{(j)}}{\sum_{j=1} w_t^{(j)}} \right)^2 \right)^{-1}, \tag{33}$$

is lower than a threshold N_{ESS}. The steps of the proposed SM-SVSF are summarized in Algorithm 2. For the SVA-IS implementation, we consider Radial Basis Function (RBF) kernel [28], [32].

We now report the computational complexity for the SM-SVSF method. Sampling the sight condition $\{\mathbf{m}_t\}_{j=1}^{N_p}$ has a complexity in the order of $\mathcal{O}(N \cdot N_p)$. At each iteration ℓ, the complexity of the SVA-IS algorithm is then:

$$\mathcal{O}(N_m \cdot \nu_m + N_p \cdot N_m \cdot \nu_k + (N_p - N_m) \cdot \nu_\alpha), \tag{34}$$

where ν_m is the cost of computing the gradient in (26), ν_k is the cost of evaluating the kernel and its gradient, and ν_α is the cost of computing the weight in (22). The kernel evaluation cost ν_k is linearly proportional to the state dimension $\tilde{d}$. The weight computation involves a determinant calculation, making $\nu_\alpha = \mathcal{O}(\tilde{d}^3)$. Although $\tilde{d} = 2$ in our setting, making the cost relatively low, the computational burden can be further reduced to $\mathcal{O}(\tilde{d})$ using determinant approximation techniques as suggested in [52]. Finally, the gradient computation has a complexity of $\nu_m = \mathcal{O}(N - 1 + \tilde{d}^2)$ due to the calculation of the log-likelihood gradient $\mathcal{O}(N-1)$ and the log-prior gradient $\mathcal{O}(\tilde{d}^2)$. The memory complexity of the SVA-IS algorithm is given by:

$$\mathcal{O}(2 \cdot N_p \cdot (\tilde{d} + N)) + N_m \cdot \tilde{d} + 2 \cdot (N_p - N_m)), \tag{35}$$

where $2 \cdot N_p \cdot (\tilde{d} + N)$ is the memory required for storing the state and sight condition particles at time $t-1$ and t, $N_m \cdot \tilde{d}$ accounts for the memory used to store the N_m gradients, and $2 \cdot (N_p - N_m)$ represents the memory needed to store the unnormalized and proposal weights. Considering both the computational and memory complexity, we can conclude that implementing the proposed method on a real-time embedded device is feasible, provided that a low-dimensional state and a small number of particles are used. Additionally, gradient computation can be parallelized when multi-threaded or GPU-based hardware is available.

IV. Experimental Assessment

We first introduce in Section IV-A the setup for the experimental campaigns and metrics for performance evaluation; then, we discuss about the obtained results in Section IV-B.

Algorithm 2: Switching Model Stein Variational Sampling Filter (SM-SVSF)

Input: Initial set of particles $\{\mathbf{x}_0^{(j)}, \mathbf{m}_0^{(j)}\}_{j=1}^{N_p}$
for $t = 1, \ldots, T$ **do**
  Sampling $\mathbf{m}_t^{(j)} \sim p(\mathbf{m}_t|\mathbf{m}_{t-1})$
  Sampling $\mathbf{x}_t^{(j)}$ using SVA-IS
  Compute importance weights $w_t^{(j)}$ using (29)
  Estimate current location $\widehat{\mathbf{x}}_t$ with (30)
  if ESS $\leq N_{\text{ESS}}$ **then**
    Apply systematic resampling
  end
end
Result: Set of estimated user positions $\{\widehat{\mathbf{x}}_t\}_{t=1}^{T}$

Fig. 5: Testing area at the MADE Competence Center I4.0, located at the Politecnico di Milano's Bovisa Campus. The map highlights the environment, with detailed insets showing the office area on the left and the machinery area on the right.

A. Setup and performance metrics

We present two experimental campaigns we conducted at the MADE Competence Center I4.0 in the Bovisa campus of the Politecnico di Milano, highlighted in Fig. 5. The first one takes place in the indoor office area shown on the bottom-left of Fig. 5, while the second one occurs in the machinery area depicted on the bottom-right. We consider these two scenarios as representative of industrial production plant conditions.

For the considered tests, we use the UWB anchors of the Just 4 Track positioning system. The UWB devices work on UWB channel 5 with a central frequency of 6489.6 MHz and a bandwidth of 499.2 MHz. The APs are wireless synchronized with the clock of the reference anchor. We use $N = 6$ APs in both the experimental campaigns. In the office experiment, a person wearing a UWB tag follows a clockwise path around a table. Ground truth positions are obtained from motion sensors placed along the path and aligned with UWB data timestamps. The experiment has been repeated five times with people moving in the room causing shadowing and signal blockage.

In this experiment, the primary source of signal blockage is the presence of humans [34], [35], which cause significant attenuation and fluctuation effects on the direct path power [58], [59]. This, paired with the dense multipath in the considered office environment, makes the perturbation significantly increase the likelihood of having the first path attenuated and early arriving multipath generating ambiguities. In [60], experimental measurements on UWB antennas showed that the presence of the human body introduces a path loss approximately 10 dB higher than in the LOS case, along with an increased TOA delay spread due to NLOS conditions. In [49], experiments under NLOS conditions caused by human shadowing showed that the TDOA error distribution exhibits a long tail extending up to 0.5 m, in contrast to the LOS error distribution. In the machinery experiments, we use an Automated Guided Vehicle (AGV) which follows a pre-programmed path at constant speed with an UWB tag mounted on its top. The NLOS in this experiment is mainly caused by metallic objects and building's structural components in the area. The surroundings and the ceiling metallic structures significantly contribute to multipath propagation. In this case, the ground truth is determined using video recordings of the test. From now on, these two tests are referred as "office test" and "AGV test". During all the executed tests, we collect TDoA data and we process them offline.

We compare the proposed filter with the bootstrap SM-PF developed in [49] by running 100 Monte Carlo simulations for each test so as to average over the random components of the tracking filters. For evaluating the filters' accuracy, we consider the 2-D position Root Mean Square Error (RMSE) (averaged over time and Monte Carlo iterations). Furthermore, we assess the robustness analysis using boxplots, considering as performance metric the upper adjacent of the position error:

$$\overline{u} = Q_3 + 1.5\,(Q_3 - Q_1), \tag{36}$$

where $Q_1 = \Pr(\left|\left|\widehat{\mathbf{x}}_t - \mathbf{x}_t\right|\right| \leq 0.25)$ is the first quartile whereas $Q_3 = \Pr(\left|\left|\widehat{\mathbf{x}}_t - \mathbf{x}_t\right|\right| \leq 0.75)$ is the third quartile.

For filter calibration, we select $\sigma_{\text{LOS}} = 0.27\,\text{m}$, $\sigma_{\text{NLOS}} = 0.39\,\text{m}$, and $\lambda = 0.41\,\text{m}^{-1}$ for the measurement noise. For the motion model in (1), the noise covariance is defined as $\mathbf{Q}_t = \sigma_{\mathbf{w}}^2 \mathbf{I}_2$. We set $\sigma_{\mathbf{w}} = 0.027\,\text{m/s}$ in the office experiment and $\sigma_{\mathbf{w}} = 0.014\,\text{m/s}$ in the AGV experiment (the AGV is moving at a lower speed). The sampling time is $\Delta t = 0.1\,\text{s}$. For the sight condition, we consider $p(m_t^{(i)} = 0|m_t^{(i)} = 0) = 0.7$ and $p(m_t^{(i)} = 1|m_t^{(i)} = 1) = 0.4$ in the office experiment, while for the AGV experiment we use $p(m_t^{(i)} = 0|m_t^{(i)} = 0) = 0.9$ and $p(m_t^{(i)} = 1|m_t^{(i)} = 1) = 0.1$. The calibration of transition probabilities has been conducted through an empirical

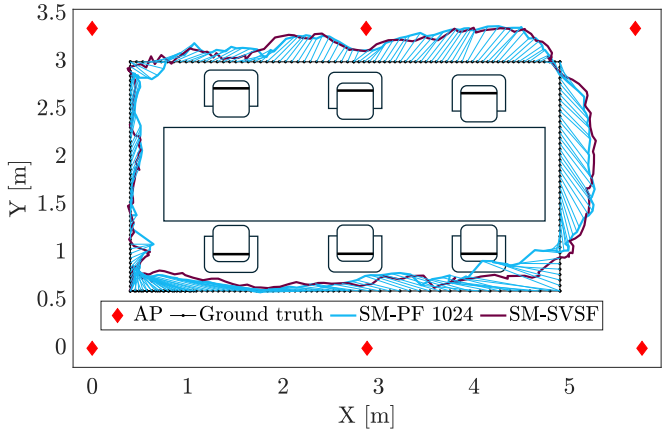

(a)

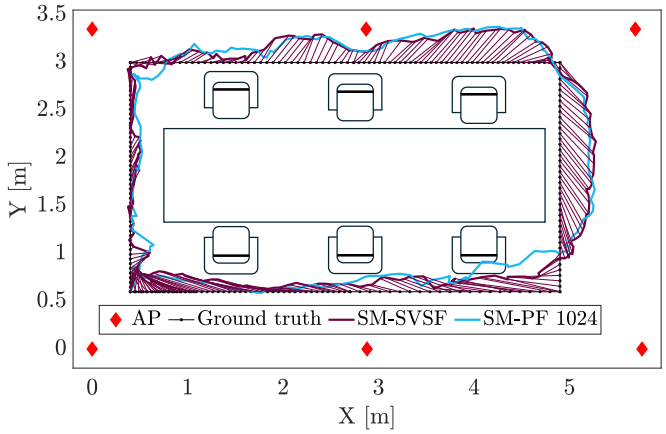

(b)

Fig. 6: Estimated trajectories in the office scenario (test 1). (a) Focus on SM-PF. (b) Focus on SM-SVSF.

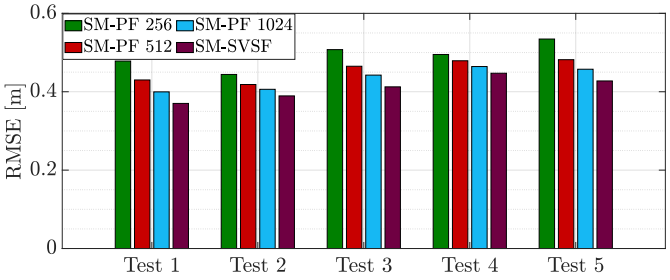

Fig. 7: Average position RMSE for the office test.

approach by iteratively evaluating the results and identifying the most suitable value based on performance metrics. The SM-PF is implemented with $N_p = \{256, 512, 1024\}$ particles. The SM-SVSF has $N_p = 256$ particles, with master particles set of size $N_m = 16$. We also set $L = 20$ iterations and a step size $\varepsilon = 0.001$ for both experiments. For gradient clipping, we select a threshold $\eta = 50$. The resampling step is executed at each time step for both SM-PF and proposed filter (i.e., we set $N_{\text{ESS}} = N_p$ for the SM-PF and $N_{\text{ESS}} = N_p - N_m$ for the SM-SVSF). At each Monte Carlo iteration, we randomly initialize the sight conditions $\{\mathbf{m}_0^{(j)}\}_{j=1}^{N_p}$ by sampling each element of $\mathbf{m}_0^{(j)}$ from a Bernoulli distribution with equally probable LOS/NLOS condition, i.e., with initial probability $p = 0.5$.

B. Numerical results

We first highlight the trajectories estimated by the proposed SM-SVSF and the SM-PF with $N_p = 1024$ during the first office experiment, as shown in Fig. 6. It can be observed that the estimates from both filters are close to the true tracks. In Fig. 7, we present the bar plot of the 2-D RMSE for all five office tests. As expected, by increasing the number of particles, the SM-PF positioning accuracy also increases. Nonetheless, the SM-SVSF outperforms the SM-PF method in all the tests, even when the latter is implemented with a higher number of particles. Moreover, the SM-SVSF is the only method that achieves an RMSE below 40 cm in both Test 1 and Test 2. These results highlight the advantage of the proposed SM-SVSF methodology, which achieves better accuracy compared to the SM-PF. Fig. 8 presents the boxplots illustrating the positioning errors across 100 Monte Carlo iterations for all the tests. Considering the upper adjacent, we observe that the SM-SVSF has worst performance with respect to the SM-PF with 1024 particles only in test 4 (Fig. 8d), where the upper adjacent of SM-PF with 1024 particles is only 0.2 cm lower than the SM-SVSF one. In other tests, the upper adjacent values of the SM-SVSF algorithm show greater improvements: for instance, in Test 2, it is 7 cm lower than the best SM-PF, and in Test 5, the improvement is 5 cm. The robustness of the two algorithms in Tests 1 and 3 are comparable. Overall, from the office test we can claim that SM-SVSF has better accuracy and slightly improved robustness with respect to SM-PF. The better accuracy results are probably due to the better sampling performed on the optimal proposal distribution by the SM-SVSF.

Concerning the AGV experiment, we compare the estimated trajectories by the proposed filter and the SM-PF with $N_p = 1024$ in Fig. 9a, while in Fig. 9b and Fig. 9c we focus on single trajectories. We can notice that the APs in the upper part of the deployment highlighted in Fig. 9a are in NLOS most of the time, since the direct path is obstructed by objects in the area. As for the office experiment, we can state that both filters are correctly tracking the AGV, even with strong NLOS conditions. The bar plot of the RMSE obtained from Monte Carlo simulations is presented in Fig. 10. In this experiment, the RMSE of the SM-SVSF is close to 10 cm and it is lower than the RMSE of all the considered SM-PF methods, which yield RMSEs of 19 cm, 16 cm and 14 cm with 256, 512 and 1024 particles, respectively. Note that the RMSE values recorded in the AGV experiment are smaller compared to those in the office scenario, primarily because the AGV's speed is lower than the typical walking speed of a human. Even in this case, the SM-SVSF achieves an accuracy better than the SM-PF, owing to sampling from the optimal proposal distribution. Similar to the office experiments, the boxplots of positioning errors for the AGV experiment across 100 Monte Carlo runs are presented in Fig. 11. Unlike the office experiment, where the SM-SVSF shows improved robustness in Tests 2 and 5 and comparable performance in the remaining tests, for the

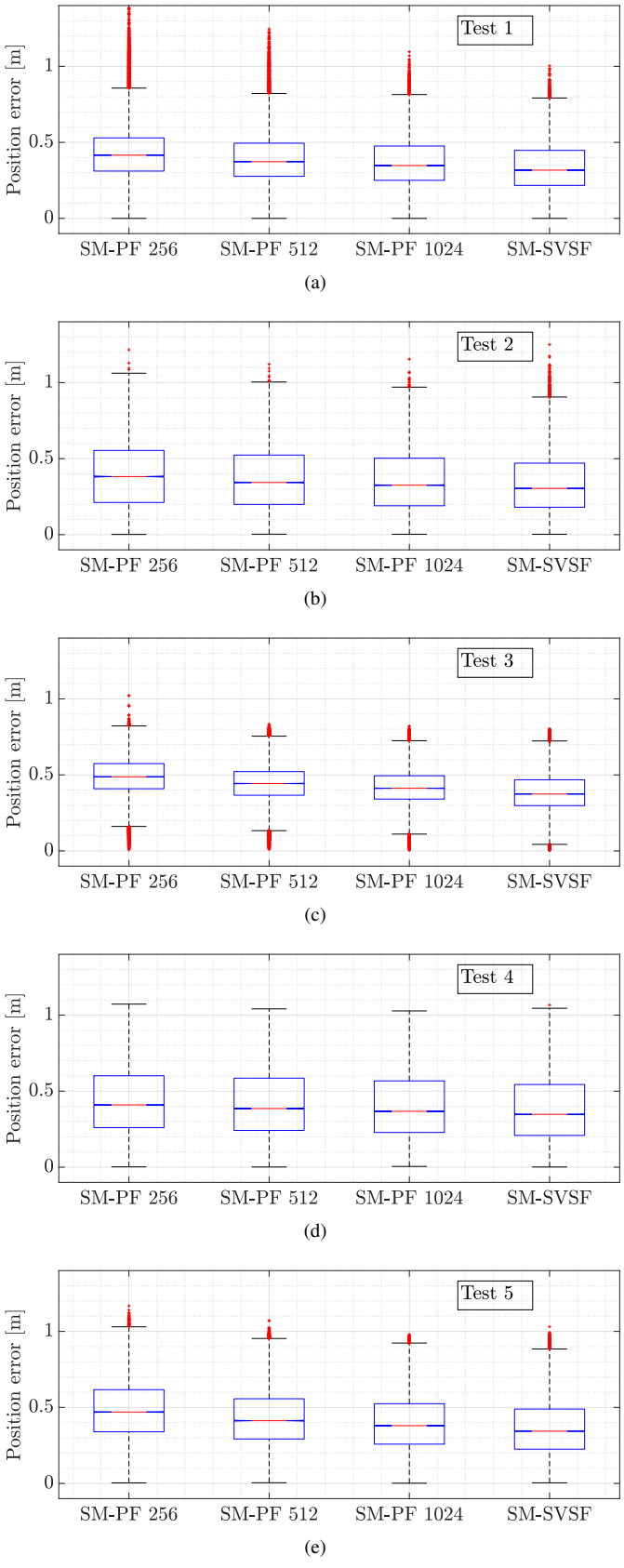

Fig. 8: Boxplots of position error in the office scenario. (a) Test 1. (b) Test 2. (c) Test 3. (d) Test 4. (e) Test 5.

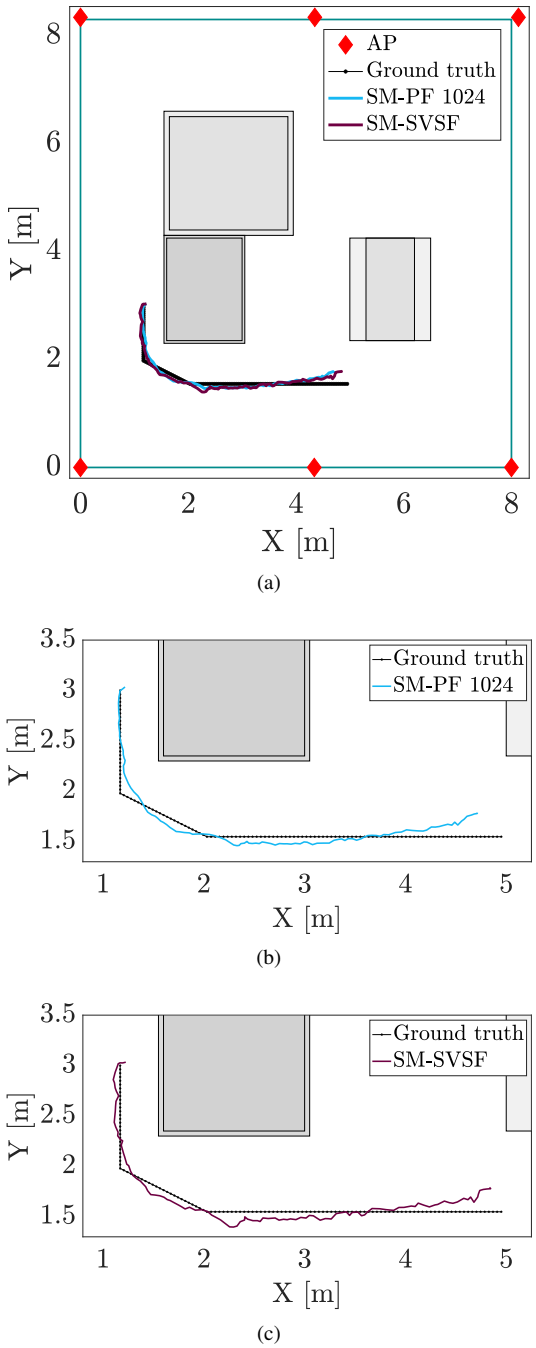

Fig. 9: Estimated trajectories in the machinery scenario. (a) Comparison of SM-PF and SM-SVSF. (b) Focus on SM-PF. (c) Focus on SM-SVSF.

AGV experiments the proposed filter outperforms the SM-PF considering the upper adjacent, which is improved by 5 cm with respect to the SM-PF with 1024 particles. To conclude, the proposed filter is able to outperforms the SM-PF in the machinery area experiment, both in terms of accuracy and robustness. The proposed SM-SVSF method effectively handles multipath and NLOS conditions caused by human presence in office environments and by objects in machinery areas. Additional experiments considering more complex industrial scenarios, such as larger spaces with harsher NLOS sources,

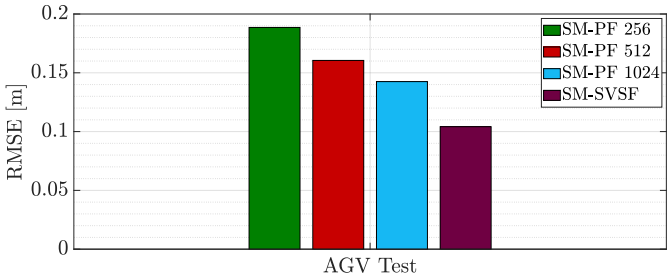

Fig. 10: Average position RMSE for the AGV test.

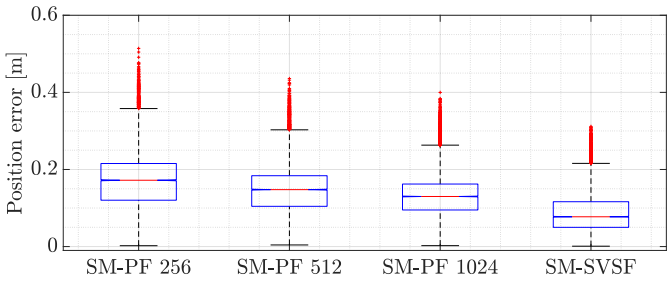

Fig. 11: Boxplots of position error in the AGV test.

including walls, machines, and time-varying obstructions like humans and moving robots, would represent a valuable asset to strengthen the claims presented in this article.

V. Conclusion

This article addressed the problem of indoor localization in mixed LOS/NLOS conditions using the UWB technology. We proposed a novel Bayesian filter based on the SVA-IS framework to efficiently sample from the optimal proposal distribution in non-linear and non-Gaussians switching state space models. We evaluated our solution using raw TDoA data collected during two experimental campaigns conducted in indoor environments: an office scenario and an industrial machinery area. We compared the proposed SM-SVSF with the switching PF introduced in [49], using the RMSE of the location estimate as accuracy metric, along with the upper adjacent values and boxplots to evaluate its robustness. Our experimental results demonstrated the effectiveness of the proposed SM-SVSF, which was able to outperform the PF in terms of accuracy and robustness in both the conducted experimental campaigns.

Future research directions can be oriented to extend the assessment in industrial scenarios with new technologies such as 5G or Wi-Fi. Moreover, new experiment in more complex indoor environment with stronger NLOS conditions (walls, human worker, mobile robots) will be considered in order to corroborate the results obtained by the SM-SVSF in our experiments. Finally, data fusion with different navigation technologies (like inertial sensors or Global Navigation Satellite System (GNSS)) can be considered for extending the developed algorithm to outdoor environment with challenging NLOS conditions (e.g., urban environments).

From the methodological standpoint, the filter can further improve the sampling from the optimal proposal distribution considering a gradient free SVGD framework [61] adapted to mixed discrete and continuous distributions or enhancements introduced using model based deep learning methodologies such as deep unfolding [62] as proposed in [63].

References

[1] F. Zafari, A. Gkelias, and K. K. Leung, "A survey of indoor localization systems and technologies," *IEEE Communications Surveys & Tutorials*, vol. 21, no. 3, pp. 2568–2599, 2019.

[2] P. S. Farahsari, A. Farahzadi, J. Rezazadeh, and A. Bagheri, "A survey on indoor positioning systems for IoT-based applications," *IEEE Internet of Things Journal*, vol. 9, no. 10, pp. 7680–7699, 2022.

[3] L. Bai, F. Ciravegna, R. Bond, and M. Mulvenna, "A low cost indoor positioning system using bluetooth low energy," *IEEE Access*, vol. 8, pp. 136 858–136 871, 2020.

[4] X. Feng, K. A. Nguyen, and Z. Luo, "A Wi-Fi RSS-RTT indoor positioning model based on dynamic model switching algorithm," *IEEE Journal of Indoor and Seamless Positioning and Navigation*, vol. 2, pp. 151–165, 2024.

[5] F. U. Khan, M. Awais, M. B. Rasheed, B. Masood, and Y. Ghadi, "A comparison of wireless standards in IoT for indoor localization using LoPy," *IEEE Access*, vol. 9, pp. 65 925–65 933, 2021.

[6] W. Fang, C. Xie, and B. Ran, "An accurate and real-time commercial indoor localization system in LTE networks," *IEEE Access*, vol. 9, pp. 21 167–21 179, 2021.

[7] L. Italiano, B. Camajori Tedeschini, M. Brambilla, H. Huang, M. Nicoli, and H. Wymeersch, "A tutorial on 5G positioning," *IEEE Communications Surveys & Tutorials*, vol. 27, no. 3, pp. 1488–1535, 2025.

[8] B. Wang, Y. Xu, S. Li, X. Tan, and G. Battistelli, "Indoor localization with distributed 5G small cells considering time alignment errors," *IEEE Sensors Journal*, vol. 24, no. 13, pp. 20 813–20 823, 2024.

[9] D. Porcino and W. Hirt, "Ultra-wideband radio technology: potential and challenges ahead," *IEEE Communications Magazine*, vol. 41, no. 7, pp. 66–74, 2003.

[10] K. Bregar, "Indoor UWB positioning and position tracking data set," *Scientific Data*, vol. 10, no. 1, p. 744, 2023.

[11] D. Dardari, A. Conti, U. Ferner, A. Giorgetti, and M. Z. Win, "Ranging with ultrawide bandwidth signals in multipath environments," *Proceedings of the IEEE*, vol. 97, no. 2, pp. 404–426, 2009.

[12] M. Elsanhoury *et al.*, "Precision positioning for smart logistics using ultra-wideband technology-based indoor navigation: A review," *IEEE Access*, vol. 10, pp. 44 413–44 445, 2022.

[13] D. Coppens, A. Shahid, S. Lemey, B. Van Herbruggen, C. Marshall, and E. De Poorter, "An overview of UWB standards and organizations (IEEE 802.15.4, FiRa, Apple): Interoperability aspects and future research directions," *IEEE Access*, vol. 10, pp. 70 219–70 241, 2022.

[14] S. Bottigliero, D. Milanesio, M. Saccani, and R. Maggiora, "A low-cost indoor real-time locating system based on TDOA estimation of UWB pulse sequences," *IEEE Transactions on Instrumentation and Measurement*, vol. 70, pp. 1–11, 2021.

[15] M. Piavanini *et al.*, "A self-calibrating localization solution for sport applications with UWB technology," *Sensors*, vol. 22, no. 23, 2022.

[16] M. Piavanini *et al.*, "A calibration method for antenna delay estimation and anchor self-localization in UWB systems," in *2022 IEEE International Workshop on Metrology for Industry 4.0 & IoT (MetroInd4.0&IoT)*, 2022, pp. 173–177.

[17] C. L. Sang, M. Adams, M. Hesse, and U. Rückert, "Bidirectional UWB localization: A review on an elastic positioning scheme for gnss-deprived zones," *IEEE Journal of Indoor and Seamless Positioning and Navigation*, vol. 1, pp. 161–179, 2023.

[18] L. Taponecco, A. D'Amico, and U. Mengali, "Joint TOA and AOA estimation for UWB localization applications," *IEEE Transactions on Wireless Communications*, vol. 10, no. 7, pp. 2207–2217, 2011.

[19] G. K. Fischer *et al.*, "A systematic survey and comparative analysis of angular-based indoor localization and positioning technologies," *IEEE Communications Surveys & Tutorials*, pp. 1–1, 2025.

[20] C. Steiner and A. Wittneben, "Low complexity location fingerprinting with generalized UWB energy detection receivers," *IEEE Transactions on Signal Processing*, vol. 58, no. 3, pp. 1756–1767, 2010.

[21] M. Stahlke, T. Feigl, S. Kram, B. M. Eskofier, and C. Mutschler, "Uncertainty-based fingerprinting model monitoring for radio localization," *IEEE Journal of Indoor and Seamless Positioning and Navigation*, vol. 2, pp. 166–176, 2024.

[22] F. Daum, "Nonlinear filters: beyond the Kalman filter," *IEEE Aerospace and Electronic Systems Magazine*, vol. 20, no. 8, pp. 57–69, 2005.

[23] E. Wan and R. Van Der Merwe, "The unscented Kalman filter for nonlinear estimation," in *Proceedings of the IEEE 2000 Adaptive Systems for Signal Processing, Communications, and Control Symposium (Cat. No.00EX373)*, 2000, pp. 153–158.

[24] I. Arasaratnam and S. Haykin, "Cubature Kalman filters," *IEEE Transactions on Automatic Control*, vol. 54, no. 6, pp. 1254–1269, 2009.

[25] Á. F. García-Fernández, L. Svensson, M. R. Morelande, and S. Särkkä, "Posterior linearization filter: Principles and implementation using sigma points," *IEEE Transactions on Signal Processing*, vol. 63, no. 20, pp. 5561–5573, 2015.

[26] A. Doucet and A. Johansen, "A tutorial on particle filtering and smoothing: Fifteen years later," *Handbook of Nonlinear Filtering*, vol. 12, 2009.

[27] Y. Shen, B. Hwang, and J. P. Jeong, "Particle filtering-based indoor positioning system for beacon tag tracking," *IEEE Access*, vol. 8, pp. 226 445–226 460, 2020.

[28] Q. Liu and D. Wang, "Stein variational gradient descent: A general purpose Bayesian inference algorithm," in *NIPS*, 2016, pp. 3115–3123.

[29] Q. Liu, "Stein variational gradient descent as gradient flow," in *Advances in Neural Information Processing Systems*, I. Guyon *et al.*, Eds., vol. 30. Curran Associates, Inc., 2017.

[30] F. D'Angelo and V. Fortuin, "Annealed stein variational gradient descent," in *Third Symposium on Advances in Approximate Bayesian Inference*, 2021.

[31] F. A. Maken, F. Ramos, and L. Ott, "Stein particle filter for nonlinear, non-Gaussian state estimation," *IEEE Robotics and Automation Letters*, vol. 7, no. 2, pp. 5421–5428, 2022.

[32] M. Piavanini, L. Barbieri, M. Brambilla *et al.*, "Annealed stein particle filter for mobile positioning in indoor environment," in *2023 IEEE International Conference on Communications (ICC)*, 2023, pp. 1–6.

[33] H. B. Lim, D. Baumann, and E.-P. Li, "A human body model for efficient numerical characterization of UWB signal propagation in wireless body area networks," *IEEE Transactions on Biomedical Engineering*, vol. 58, no. 3, pp. 689–697, 2011.

[34] Q. Tian, K. I.-K. Wang, and Z. Salcic, "Human body shadowing effect on UWB-based ranging system for pedestrian tracking," *IEEE Transactions on Instrumentation and Measurement*, vol. 68, no. 10, pp. 4028–4037, 2019.

[35] Y. Geng, J. He, and K. Pahlavan, "Modeling the effect of human body on TOA based indoor human tracking," *International Journal of Wireless Information Networks*, vol. 20, no. 4, pp. 306–317, 2013.

[36] I. Guvenc and C.-C. Chong, "A survey on TOA based wireless localization and NLOS mitigation techniques," *IEEE Communications Surveys & Tutorials*, vol. 11, no. 3, pp. 107–124, 2009.

[37] R. Mendrzik, H. Wymeersch, G. Bauch, and Z. Abu-Shaban, "Harnessing NLOS components for position and orientation estimation in 5G millimeter wave MIMO," *IEEE Transactions on Wireless Communications*, vol. 18, no. 1, pp. 93–107, 2019.

[38] J. Xie, W. Wang, X. Liu, I. Rashdan, C. Di, and J. Qin, "Identification of NLOS based on soft decision method," *IEEE Wireless Communications Letters*, vol. 12, no. 4, pp. 703–707, 2023.

[39] C. Jiang, J. Shen, S. Chen, Y. Chen, D. Liu, and Y. Bo, "UWB NLOS/LOS classification using deep learning method," *IEEE Communications Letters*, vol. 24, no. 10, pp. 2226–2230, 2020.

[40] J. Ott, M. Stahlke, T. Feigl, and C. Mutschler, "Estimating multipath component delays with transformer models," *IEEE Journal of Indoor and Seamless Positioning and Navigation*, vol. 2, pp. 219–229, 2024.

[41] B. Camajori Tedeschini and M. Nicoli, "Cooperative deep-learning positioning in mmwave 5G-advanced networks," *IEEE Journal on Selected Areas in Communications*, vol. 41, no. 12, pp. 3799–3815, 2023.

[42] S. Yi and M. Zorzi, "Robust Kalman filtering under model uncertainty: The case of degenerate densities," *IEEE Transactions on Automatic Control*, vol. 67, no. 7, pp. 3458–3471, 2022.

[43] X. Zhu, J. Yi, J. Cheng, and L. He, "Adapted error map based mobile robot UWB indoor positioning," *IEEE Transactions on Instrumentation and Measurement*, vol. 69, no. 9, pp. 6336–6350, 2020.

[44] H. Nurminen, T. Ardeshiri, R. Pich, and F. Gustafsson, "Robust inference for state-space models with skewed measurement noise," *IEEE Signal Processing Letters*, vol. 22, no. 11, pp. 1898–1902, 2015.

[45] Y. Huang, Y. Zhang, Y. Zhao, L. Mihaylova, and J. A. Chambers, "Robust Rauch-Tung-Striebel smoothing framework for heavy-tailed and/or skew noises," *IEEE Transactions on Aerospace and Electronic Systems*, vol. 56, no. 1, pp. 415–441, 2020.

[46] B. Cao, S. Wang, S. Ge, and W. Liu, "Improving the positioning accuracy of UWB system for complicated underground NLOS environments," *IEEE Systems Journal*, vol. 16, no. 2, pp. 1808–1819, 2022.

[47] Y. Zhang, W. Fu, D. Wei, J. Jiang, and B. Yang, "Moving target localization in indoor wireless sensor networks mixed with LOS/NLOS situations," *EURASIP Journal on Wireless Communications and Networking*, vol. 2013, p. 291, 2013.

[48] Y. El-Laham, L. Yang, P. M. Djurić, and M. F. Bugallo, "Particle filtering under general regime switching," in *2020 28th European Signal Processing Conference (EUSIPCO)*, 2021, pp. 2378–2382.

[49] L. Barbieri, M. Brambilla, A. Trabattoni, S. Mervic, and M. Nicoli, "UWB localization in a smart factory: Augmentation methods and experimental assessment," *IEEE Transactions on Instrumentation and Measurement*, vol. 70, pp. 1–18, 2021.

[50] F. Gustafsson *et al.*, "Particle filters for positioning, navigation, and tracking," *IEEE Transactions on Signal Processing*, vol. 50, no. 2, pp. 425–437, 2002.

[51] Á. F. García-Fernández, R. Hostettler, and S. Särkkä, "Rao-Blackwellized posterior linearization backward SLAM," *IEEE Transactions on Vehicular Technology*, vol. 68, no. 5, pp. 4734–4747, 2019.

[52] J. Han and Q. Liu, "Stein variational adaptive importance sampling," *arXiv: Machine Learning*, 2017.

[53] A. F. Molisch, "Ultra-wide-band propagation channels," *Proceedings of the IEEE*, vol. 97, no. 2, pp. 353–371, 2009.

[54] T. Li, M. Bolic, and P. M. Djuric, "Resampling methods for particle filtering: Classification, implementation, and strategies," *IEEE Signal Processing Magazine*, vol. 32, no. 3, pp. 70–86, 2015.

[55] Y. Zhang, R. Wang, and Z. Xing, "A robust evolutionary particle filter technique for integrated navigation in urban environments via GNSS and 5G signals," *IEEE Transactions on Industrial Informatics*, vol. 20, no. 4, pp. 6866–6878, 2024.

[56] K. P. Murphy, *Probabilistic Machine Learning: An introduction*. MIT Press, 2022.

[57] P. Blanchard, D. J. Higham, and N. J. Higham, "Accurately computing the log-sum-exp and softmax functions," *IMA Journal of Numerical Analysis*, vol. 41, no. 4, pp. 2311–2330, 5/20/2025 2021.

[58] S. Savazzi, M. Nicoli, F. Carminati, and M. Riva, "A Bayesian approach to device-free localization: Modeling and experimental assessment," *IEEE Journal of Selected Topics in Signal Processing*, vol. 8, no. 1, pp. 16–29, 2014.

[59] V. Rampa, S. Savazzi, M. Nicoli, and M. DAmico, "Physical modeling and performance bounds for device-free localization systems," *IEEE Signal Processing Letters*, vol. 22, no. 11, pp. 1864–1868, 2015.

[60] R. Bharadwaj and S. K. Koul, "Study of the influence of human subject on the indoor channel using compact UWB directive/omni-directional antennas for wireless sensor network applications," *Ad Hoc Networks*, vol. 118, p. 102521, 2021.

[61] J. Han and Q. Liu, "Stein variational gradient descent without gradient," in *Proceedings of the 35th International Conference on Machine Learning*, ser. Proceedings of Machine Learning Research, J. Dy and A. Krause, Eds., vol. 80. PMLR, 2018, pp. 1900–1908.

[62] V. Monga, Y. Li, and Y. C. Eldar, "Algorithm unrolling: Interpretable, efficient deep learning for signal and image processing," *IEEE Signal Processing Magazine*, vol. 38, no. 2, pp. 18–44, 2021.

[63] M. Piavanini, L. Barbieri, M. Brambilla, and M. Nicoli, "Deep unfolded annealed stein particle filter for vehicle tracking," in *ICASSP 2024 - 2024 IEEE International Conference on Acoustics, Speech and Signal Processing (ICASSP)*, 2024, pp. 13 226–13 230.

Marco Piavanini (Graduate Student Member, IEEE) received the B.Sc. in biomedical engineering and the M.Sc. in telecommunication engineering from the Politecnico di Milano in 2017 and 2021, respectively. In November 2021, he started his Ph.D. in information technology at the Politecnico di Milano. His research interests include Bayesian filters and deep learning for localization in wireless networks, with applications in automotive and indoor industrial settings.

Mattia Brambilla (Member, IEEE) received the B.Sc. and M.Sc. degrees in telecommunication engineering and the Ph.D. degree (cum laude) in information technology from the Politecnico di Milano, in 2015, 2017, and 2021, respectively. He was a visiting researcher with the NATO Centre for Maritime Research and Experimentation (CMRE), La Spezia, Italy, in 2019. In 2021, he joined the faculty of Dipartimento di Elettronica, Informazione e Bioingegneria (DEIB) at the Politecnico di Milano as Research Fellow. His research interests include signal processing, statistical learning, and data fusion for cooperative localization and communication. He is an Associate Editor for the IEEE Open Journal of Signal Processing. He was a recipient of the Best Student Paper Award at the 2018 IEEE Statistical Signal Processing Workshop.

Monica Nicoli (Senior Member, IEEE) received the M.Sc. (Hons.) and Ph.D. degrees in communication engineering from Politecnico di Milano, Milan, Italy, in 1998 and 2002, respectively. She was a Visiting Researcher with ENI Agip, from 1998 to 1999, and Uppsala University, in 2001. In 2002, she joined Politecnico di Milano as a Faculty Member. She is currently an Associate Professor in telecommunications with the Department of Management, Economics and Industrial Engineering. Her research interests include signal processing, machine learning, and wireless communications, with emphasis on smart mobility and Internet of Things (IoT) applications. She was a recipient of the Marisa Bellisario Award, in 1999, and a co-recipient of the best paper awards of the IEEE Symposium on Joint Communications and Sensing, in 2021, the IEEE Statistical Signal Processing Workshop, in 2018, and the IET Intelligent Transport Systems journal, in 2014. She is an Associate Editor of the IEEE Transactions on Intelligent Transportation Systems.